




RESEARCH ARTICLE

Analysis of High Temperature Motors With Micro-Arc Oxidation Ceramic Insulated Wire

WANG LIANKE¹, (Student Member, IEEE), FU DONGSHAN¹, (Member, IEEE),
WANG XIANGRUI¹, ZHOU YONG², SI HONGYU², GENG YINGSAN¹, (Senior Member, IEEE),
LEI LI³, AND XIANG BO²

¹State Key Laboratory of Electrical Insulation and Power Equipment, Xi'an Jiaotong University, Xi'an 710049, China

²School of Electrical Engineering, China University of Mining and Technology, Xuzhou 221116, China

³Kunshan Sino-Russian Joint New Materials Research Center, Kunshan 215332, China

Corresponding author: Fu Dongshan (fudongshan@outlook.fr)

This work was supported in part by the State Key Laboratory of Electrical Insulation and Power Equipment under Grant EIPE23212.

ABSTRACT The use of organic insulation in the motor has insulation temperature limitations, which limit its usage and further increase its power density. In response to this issue, this paper proposes a high-temperature resistant motor with the micro-arc oxidation ceramic insulated wire, of which the long-term service temperature is able to exceed 350 °C. Firstly, the generation conditions, formation principles, structural characteristics and electrical characteristics of micro-arc oxidation ceramic insulated wires were introduced. Secondly, the high temperature motor base on micro-arc oxidation ceramic insulated wires is proposed, and the temperature analysis is presented, the influence of motor load on temperature rise was studied. Then, the manufacturing process and insulation method of the motor were introduced. Finally, the high-temperature motor prototype was made, and the high-temperature resistance performance of the high-temperature motor prototype was tested, and the temperature distribution of the motor under different load conditions was verified.


INDEX TERMS Micro-arc oxidation, ceramic insulated wire, high-temperature resistant motor.

I. INTRODUCTION

The replacement of primary energy sources such as oil by electricity has become a trend in the automotive, rail transportation, and aviation sectors [1], which places higher demands on the power density of electric motors. The current density in the active conductor in the motor affects the power density of the motor [2], while the maximum current density is determined by the operating temperature of the Electrical Insulation System (EIS) and the cooling system [3]. Motor designs have typically improved power density by changing the cooling approaches from forced air cooling towards indirect Water& Glycol (WG) based jacket cooling approaches, and by applying more direct water or oil-based coil-cooling methods [4], [5], [6]. However, the cooling system can

only partially dissipate the heat inside the motor and cannot fundamentally improve the temperature tolerance of the motor.

Motor temperature tolerance is governed by the motor's internal EIS, and once the temperature exceeds the thermal decomposition temperature of the EIS, the insulation materials rapidly lose their dielectric properties [7]. Most motors used in high power density applications are now made with organic enameled wire. However, the organic EIS has a limited operating temperature depending on the expected lifetime. The standard organic enameled wires have a thermal class of 180 or 200 °C. More expensive enameled wires based on polyimide (PI) coating have a thermal class of 240 °C. The motor with organic EIS works at higher temperatures for a very short time which makes them available only for very specific applications such as high temperature fume extractor and electric torpedo [8], and for some

The associate editor coordinating the review of this manuscript and approving it for publication was Guillaume Parent .

continuous high temperature application scenarios, such as near aircraft turbines, the ambient temperature already reaches 350 °C. The organic EIS cannot withstand such high temperature.

To improve the power density of motor and their ability to withstand high temperature environments, the higher temperature (HT^o) EIS especially inorganic EIS is put forward. An electrical machine made with inorganic rigid coils to breakthrough toward high temperature motors for aeronautics is present in [3]. The inorganic rigid coils are mainly made of copper which is protected from oxidation by a layer of nickel, on the nickel layer, a thin ceramic layer is deposited. The wire is able to operate permanently at 500 °C. However, the dielectric properties of ceramic wire at high temperatures are relatively poor. To overcome the problem, a dip coating with boron oxide is used to improve insulation quality of the ceramic insulated conductors in [9], a dip coating was employed to apply Low Temperature Co-firing Ceramic (LTCC) zinc molybdate coatings to the surfaces of Ni-coated Cu conductor wires is presented in [10]. The ceramic insulated wires mentioned above are based on Ni-coated Cu conductor wires and a ceramic layer depositing outside, which is hard to pliant. Inorganic coils applied to motors must adapt to the physical properties of inorganic HT^o coils as rigid objects, so the stator must be designed as rectangular opened teeth to be assembled, which is quite different from the semi-closed slots of ordinary motors [11]. And the rectangular opened teeth have the disadvantage of high harmonic magnet field. And the fill factor is limited by the rigid object winding. An anodized aluminum strip was proposed in [1], integrating aluminum strip in motor coils with only alumina, growth by anodization, as inter-turn insulation. This would allow making more lightweight and possibly higher temperature running motors. And a comparison between ceramic-coated wires and anodized aluminum strips used for high temperature machine is presented in [12]. It illustrates that the anodized aluminum technology offers a better filling and both the Ni-coated Cu conductor wires and anodized aluminum strips are able to increase strongly the power density. However, due to the aluminum oxide fragility, the alumina layer is very prone to cracks, the anodized alumina wire process is not suitable for round aluminum wire. Moreover, both the Ni-coated Cu conductor wires and anodized aluminum strips require a special stator construction with rectangular teeth shape and open slots. The coils have a rectangular cross section. The slots are cuboid and the teeth faces are parallel. Consequently, the slots have a specific shape with a larger width in their bottom that cannot be used by the coils.

Recently, inorganic-organic hybrid nanocomposites have attracted special attention because they can have some of the properties of both organic and inorganic. In [13], composite coatings comprising of particulate ceramic and silicon containing inorganic-organic nano-hybrids are synthesized. Incorporation of organic moiety introduces mechanical flexibility to the inorganic molecular networks [14], and at the

same time reduces thermal stability of resulting nano-hybrid materials.

In order to solve the problem mentioned above, a novel HT^o motor based Micro-arc oxidation (MAO) ceramic film on aluminum winding is proposed in this paper. This article is organized as follows. In section II, the MAO ceramic aluminum wire is introduced, the characteristics include generation conditions, formation principles, structural characteristics and electrical characteristics of the wire are investigated. In the section III, the structure of HT^o motor based on MAO ceramic insulated aluminum winding is introduced, the mathematical model for thermal analysis is proposed. In section IV, the prototype of HT^o motor is manufactured, experiments are performed to verify the thermal analysis of the motor, and followed by conclusion in Section V.

II. MAO CERAMIC INSULATED WIRE

A. THE MAO CERAMIC ALUMINUM WIRE

MAO, also known as plasma electrolytic oxidation, is a surface modification technique used to form ceramic coatings on valve metal surfaces. When conducting the MAO process on aluminum wires, a ceramic layer mainly composed of inorganic Al₂O₃ phase is able to be in-situ transformed on its surface [15], [16], [17]. The Al₂O₃ ceramic layer has high-temperature stability, good thermal conductivity, and excellent electrical insulation performance. Therefore, applying MAO technology to the aluminum wire can prepare a high-temperature-resistant electrical insulation layer on its surface. The schematic diagram of the MAO technology is shown in Fig. 1, usually using the aluminum wire as the anode and the stainless steel as the cathode. Before processing, immerse the anode and cathode in a preconfigured electrolyte, and the process is carried out under external power and cooling conditions. The aluminum MAO film layer is made of Al₂O₃ phase as the main component, which keep the phase structure and chemical composition stable up to 550 °C [16], [18].

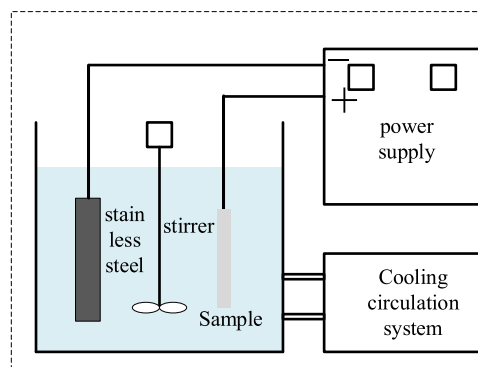


FIGURE 1. The schematic diagram of the MAO technology.

In this paper, the aluminum wire with a diameter of 1.2mm was used for samples, and a bipolar pulsed current generator



FIGURE 2. The appearance of the processed MAO ceramic insulated wire.

was used as the MAO power supply, which output the following constant parameters: a pulse frequency of 200 Hz, positive and negative pulse durations of 2 ms, and equal pulse pauses. The electrolyte used was composed of KOH and Na_2SiO_3 , which were diluted in deionized water. Its resulting electric conductivity and pH were $\sim 9.56 \text{ mS}\cdot\text{cm}^{-1}$ and ~ 12.01 , respectively. The processed sample was shown in Fig. 2, from which a white ceramic layer was prepared on the aluminum wire.

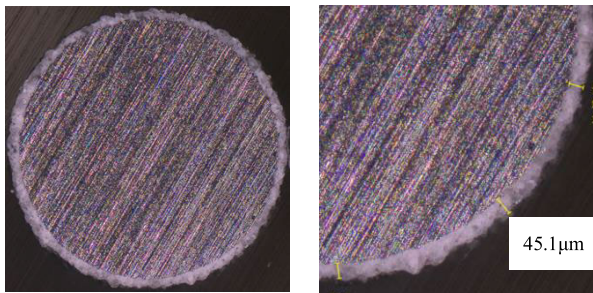


FIGURE 3. The cross section of the MAO ceramic insulated wire.

Fig. 3 shows the cross-sectional area of MAO ceramic insulated aluminum wires, with a thickness of approximately $45.1 \mu\text{m}$ for the alumina ceramic layer. The temperature limit will be determined by the aluminum melting point of approximately 660°C . Alumina melts at 2072°C , which is far from the classical limit temperature of commonly used organic varnish. The breakdown strength of ceramic coatings in air ranges from 22.9 to $47.8 \text{ kV}/\text{mm}$, which is the same as that of epoxy resin ($20 \text{ kV}/\text{mm}$) and NOMEX paper ($18 \text{ kV}/\text{mm} \sim 40 \text{ kV}/\text{mm}$) [19].

Aluminum oxide has the characteristics of high hardness and strong brittleness. When applied to motor windings, it is necessary to enhance the toughness of MAO ceramic insulated wires in order to facilitate the winding of winding coils. Using MAO technology, the aluminum surface can be oxidized to form a composite structure containing gaps and aluminum oxide, achieving insulation while maintaining a certain degree of mechanical flexibility. The Electron microscope of MAO ceramic insulated wires is shown in Fig. 4. The surface of the MAO ceramic insulated wire with gap is

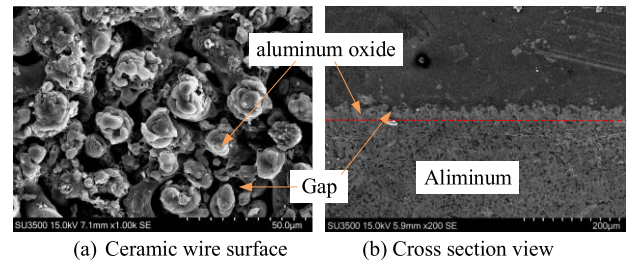


FIGURE 4. Electron microscope of the MAO ceramic insulated wire.

shown in Fig. 4 (a) and the cross section view of the MAO ceramic coating aluminum wire is shown in Fig. 4 (b).

B. COMPARISON WITH OTHER INORGANIC INSULATION

The bonding force between the ceramic surface and the inner conductor of the existing ceramic insulated wire mainly depends on the adsorption of physical forces. The bonding force is weak, and the film layer is easy to separate when subjected to stress bending. On the other hand, ceramic materials have high brittleness and lack of internal sliding system, which is prone to brittle fracture when subjected to stress deformation. When the MAO ceramic insulated wire is used as winding wire, it should bear various bending and twisting deformation while maintaining certain insulation strength. The existing ceramic insulated wires are limited by the mechanical deformation in the application scenario, so they cannot be widely used.

As for the MAO ceramic insulated wire, On the one hand, the surface ceramic and the inner conductor are bonded in the form of chemical bonds, and when the stress is bent, the film layer is closely bonded to the matrix. On the other hand, conductor aluminum has excellent flexibility and forms a lamellar composite structure with ceramic layer on the surface. Lamellar composite materials can not only maintain the performance advantages of raw materials, but also make up for the shortcomings of the two materials through “complementary effect”, which can theoretically achieve a certain degree of mechanical flexibility.

C. ELECTROMAGNETIC PROPERTIES AS APPLIED TO ELECTRICAL MACHINES

The ceramic insulated wire has the characteristics of high temperature resistance and a certain degree of flexibility, but it is also necessary to test its insulation performance and life when it is applied to the motor.

1) BREAKDOWN VOLTAGE OF MAO CERAMIC INSULATED WIRE

To obtain the power frequency breakdown voltage of MAO ceramic aluminum wire. The breakdown voltage experiment was carried out. Remove the insulation at both ends of a ceramic insulated wire sample with a length of about 400 mm, fold it in half, and twist it into a wire pair of $(125 \pm 5) \text{ mm}$ on the twisting machine. The force applied during twisting is

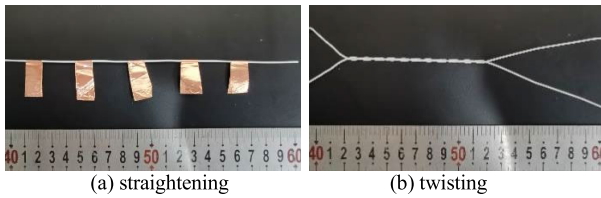


FIGURE 5. The test sample of the MAO ceramic insulated wire.

27.00N, and the number of twisting turns is 6. Then, part of the twisting end rings is cut at two places, and the distance between the ends of the cutting points is maximum. Fig. 5 shows the test sample after twisting.

A test voltage is applied between the two conductors and the voltage is increased from zero at a rate of 20V/s, using the voltage value at leakage current greater than or equal to 5mA as the breakdown voltage value. Five samples were tested in each group and five breakdown voltages were recorded. Fig. 6 shows the test results under the twisted condition. As the thickness of the film increases, the power frequency breakdown voltage also increases.

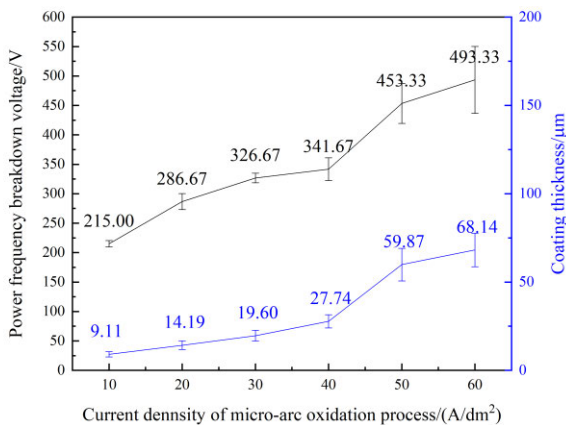


FIGURE 6. Power frequency breakdown voltage and coating thickness of ceramic insulated wires under twisted condition.

2) BREAKDOWN VOLTAGE IN HIGH TEMPERATURE

In order to further obtain the insulation performance of ceramic insulated wire in high temperature environment, high temperature resistance test was carried out. The temperature increase of MAO ceramic insulated wires in service is mainly due to the Joule heat generated by the current, which is proportional to the square of the current. For traditional organic insulated magnetic wire, when the conductor temperature exceeds the withstand temperature of the insulation material, the material will degrade and thus lose the insulation performance. Therefore, the withstand temperature of the insulation material determines the service temperature of the magnetic wire, thus limiting the upper limit of the operating temperature of related products. In order to study the insulation performance of MAO ceramic insulated wire

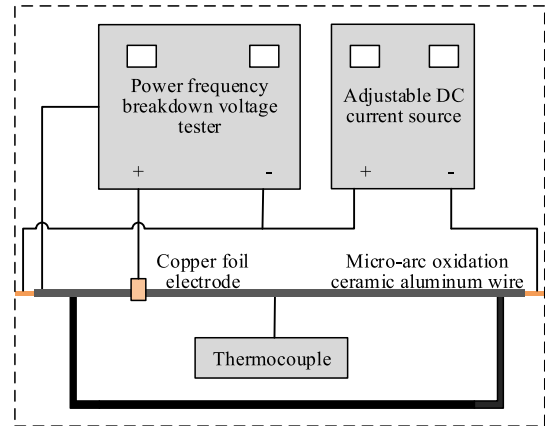


FIGURE 7. The breakdown voltage test device under the simulated high current condition.

under the condition of high temperature generated by high current, and to study the change of insulation level of ceramic layer when conductor temperature rises to different levels when high current is applied, the insulation performance was tested under high temperature environment caused by high current.

Fig. 7 shows the breakdown voltage test device under the simulated high current condition.

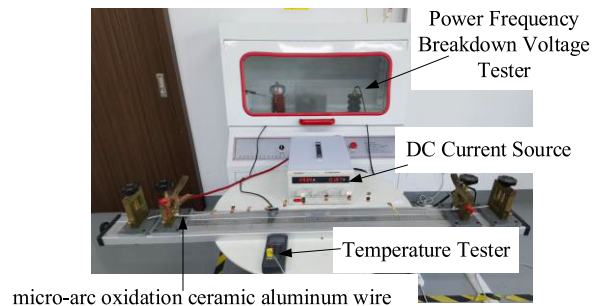


FIGURE 8. Breakdown voltage testing platform.

The two ends of the 1m long MAO ceramic insulated wire are respectively connected to the two ends of the adjustable DC constant current source. The high voltage end of the power frequency breakdown voltage instrument is directly connected with one end of the MAO ceramic insulated wire, and the copper foil at the ground end of the power frequency breakdown voltage tester is connected with the surface of the MAO ceramic insulated wire. A thermocouple is attached in the middle of the conductor to record the temperature of the conductor surface. The ceramic insulated wire is heated by passing different currents, and its temperature can be controlled by regulating the current. Fig. 9 shows the breakdown voltage at different temperature.

As Fig. 9 illustrates, with the increase of the incoming current, the conductor surface temperature rose from room temperature to 350 °C, and the power frequency breakdown

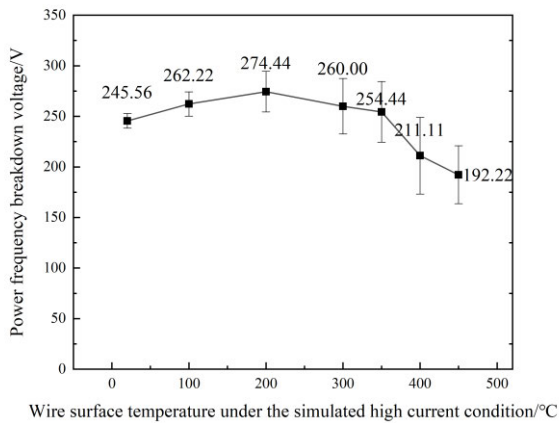


FIGURE 9. The breakdown voltage under the simulated high current condition.

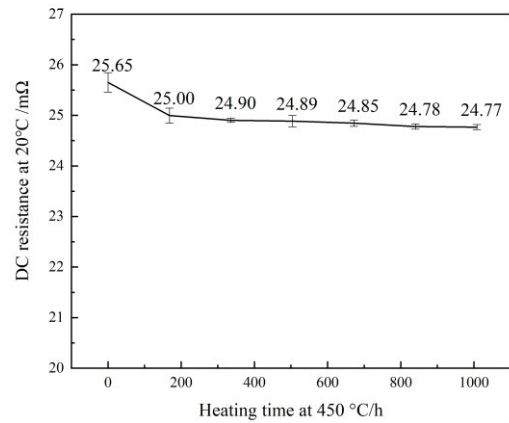


FIGURE 11. The breakdown voltage under the simulated high current condition.

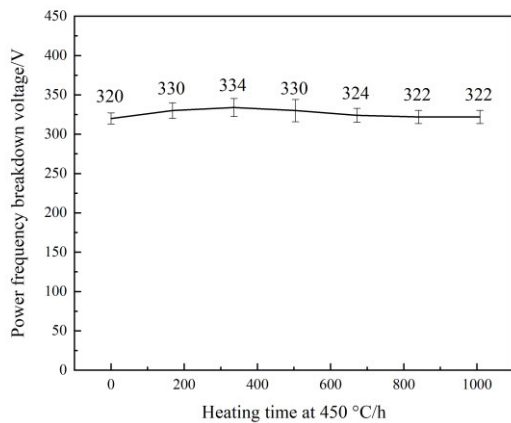


FIGURE 10. The breakdown voltage under the simulated high current condition.

voltage remained at a stable level of 250V. With the further increase of temperature, the power frequency breakdown voltage showed a downward trend.

3) IMPEDANCE STABILITY IN HIGH TEMPERATURE ENVIRONMENTS

When the surface of the conductor is heated to different high temperatures in a high-current service environment, the ceramic layer maintains corresponding insulation strength for a short period of time. However, the long-term stability of high temperature insulation performance of MAO ceramic insulated wires still needs to be further verified, which is related to the life of its practical application, and has important significance.

The MAO ceramic insulated wire with a diameter of 1.2mm was placed in a high temperature oven at 450 °C for 7 days, 14 days, 21 days, 28 days, 35 days and 42 days, respectively. The power frequency breakdown voltage of the ceramic insulated wire before and after baking was tested under twisted condition. The results are shown in Fig. 10. With the extension of the baking time to 1008h, the power

frequency breakdown voltage of the wire basically stays at 325V, indicating that the high-temperature properties of ceramic insulated wire has long-term stability.

Unlike copper conductors, which are oxidized in high temperature environments and reduce their conductivity, ceramic insulated wires have excellent long-term stability in high temperature environments. As shown in Fig. 11, the resistance of MAO ceramic insulated wires decreases by 2.53% after roasting at 450 °C for 168h, and then gradually becomes stable. The results show that the conductive properties of ceramic insulated wires have excellent long-term stability.

III. HT° MOTOR BASE ON MAO CERAMIC INSULATED WIRES

MAO ceramic insulated wire has high mechanical toughness, high temperature insulation performance and stability, so that it is suitable for motor to improve its operating temperature. However, the surface of MAO ceramic insulated wire is different from traditional organic insulated enameled wires. The surface of MAO ceramic insulated wire is relatively rough and easy to wear. Applying ceramic insulated wires to motors can achieve high temperature resistance, but their processing and manufacturing cannot be the same as traditional motors. In order to ensure the high-temperature resistance of the motor, the manufacturing process of the motor needs to be reset, and high-temperature conditions need to be considered for slot insulation, winding fixation.

In this paper, apply the MAO ceramic insulated wire to a single-phase electric excitation flux switching motor to break through the temperature limit base on the traditional enameled wire.

A. TOPOLOGY OF THE HT° MOTOR

The high temperature motor is designed as single-phase electric excitation flux switching motor and the topology is shown in Fig. 12. The motor employs four rotor poles and eight stator poles. Four fully pitch coils are mounted in stator slots, constituting two windings named as phase A and phase B which can

TABLE 1. Main structure parameters of the HT° motor.

Symbol	Quantity
Outer diameter of stator (mm)	105
inside diameter (mm)	61.6
Thickness of stator yoke (mm)	8
Outer diameter of rotor (mm)	61
Inner diameter of rotor (mm)	18
Thickness of rotor yoke (mm)	22
Winding turns of A phase	55
Winding turns of B phase	45
Stator Arc Angle (degree)	22.5
Main Air Gap Length (mm)	0.3
Rotor arc angle (degree)	44.5
Stacking thickness (mm)	36

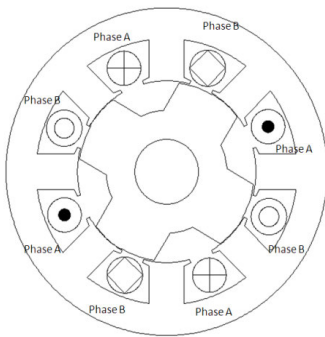


FIGURE 12. Topology of the HT° motor.

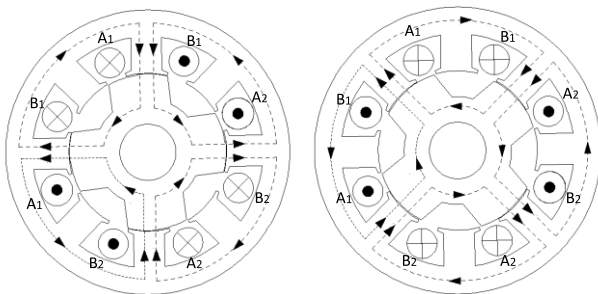


FIGURE 13. Distribution of magnetic line in different direction directions of Phase B.

features either different or the same turns of number. Phase A is the excitation phase.

According to the rotor position, the magnetic field generated by the A phase current with a single direction interacts with the electromagnetic field generated by the B phase bidirectional current to generate torque. Fig.13 shows the distribution of motor magnetic field with different directions of phase B current. The main structure parameters of the HT° motor is shown in TABLE 1. The drive topology is shown in Fig. 14 [20].

B. TEMPERATURE ANALYSIS

The motor uses a new type of insulating material, it breaks through the limitation of the temperature of the traditional motor, and the design methods and limitations of the

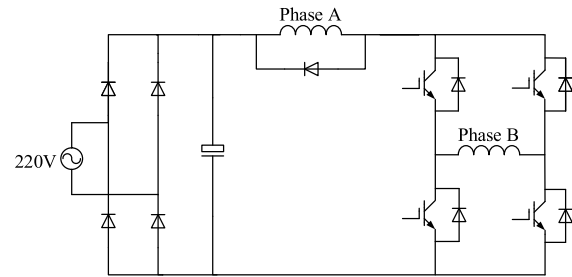


FIGURE 14. The drive topology of the HT° motor.

traditional motor are not applicable to the motor of MAO ceramic insulated wire. In order to further summarize the technical requirements of the motor design, the temperature field of the motor using the MAO ceramic insulated wire is analyzed, and the electric load of the motor under the temperature field is determined.

The thermal analysis of the motor is carried out using the fluid dynamic calculation method. The fluid dynamic mathematical model for the turbulent flow of the viscous fluid uses Reynolds-averaged Navier-Stokes equation. These equations for the steady state are as follows:

$$\nabla \bar{v} = 0 \tag{1}$$

$$\mu \nabla^2 \bar{v} = \nabla p - \rho \bar{F} + \nabla \bar{\tau} \tag{2}$$

$$\frac{\lambda}{c\rho} \nabla^2 \bar{T} + \frac{1}{c\rho} (\bar{D} + \bar{Q}) - \nabla \bar{v} \bar{T} - \nabla \bar{v}' \bar{T}' = 0 \tag{3}$$

where \bar{v} , p , \bar{T} are average values of fluid velocity, pressure and temperature separately. Q is a heat source density, $\bar{\tau}$ is reynolds stress tensor, \bar{D} is an intensity of dissipation. λ , c , ρ , μ are thermal conductivity, specific heat, mass density and dynamic viscosity respectively.

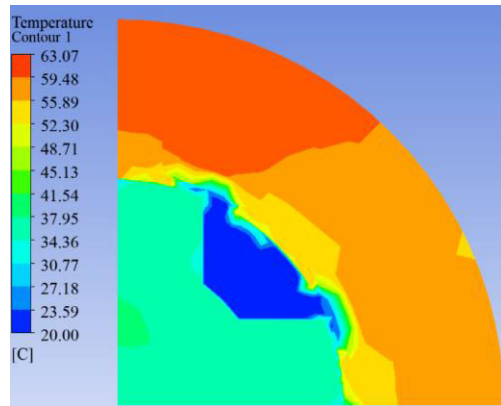
Radiation is another phenomenon which should be included in analysis for the HT° motor. The radiation inside motor can be calculated with radiation mode, for the external walls of the motor, the mixed boundary condition for energy equation (2) are used. Combined boundary condition is given by following:

$$-k \frac{\partial T}{\partial n} = h_c (T_w - T_\infty) + \varepsilon_r \sigma (T_w^4 - T_{ext}^4) \tag{4}$$

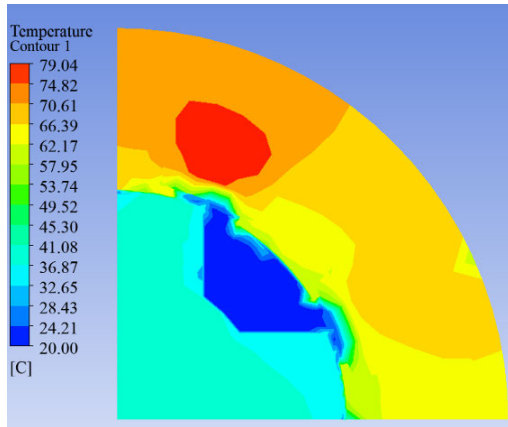
where h_c is convective heat transfer coefficient, T_∞ is temperature of the ambient air, T_w is surface temperature of the wall, T_{ext} is the ambient temperature, ε_r is the surface coefficient and σ is the Stefan-Boltzmann constant.

In order to accurately and quickly obtain the temperature field distribution of the motor. Simulate and analyze the motor using finite element method to obtain the temperature changes of the motor under different load conditions.

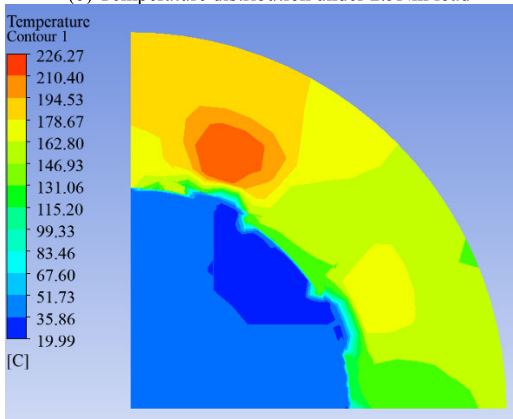
The temperature distribution of the motor under the load of 2.5Nm and 6.5Nm is shown in Fig. 15 where the ambient temperature is 20 °C, air-cooled with the speed of 10m/s. The current of the motor increases with the increase of the load, and the temperature increases with the current of the motor.



(a) Temperature distribution under 1 Nm load



(b) Temperature distribution under 2.5Nm load



(c) Temperature distribution under 6.5Nm load

FIGURE 15. Temperature distribution under different loads.

The temperature increases from 79° at a load of 2.5Nm to 226° at a load of 6.5Nm. The current, speed, and of the motor under different load conditions are shown in Table 2.

When the operating temperature of the motor increases from 75 °C to 226 °C, the output torque of the motor increases from 2.5Nm to 6.5Nm, and the power increases from 3.3kW to 6.1kW. As the temperature tolerance limit of the motor increases, both the output power and torque of the motor can

TABLE 2. Main structure parameters of the HT^o motor.

Load/ (Nm)	Phase A Current/ (A)	Phase B Current/ (A)	Speed/ (rpm)	Temperature/ (°C)
1.5	20.02	10.93	14875	66.05
2.5	27.78	18.26	12500	79.09
3.5	39.63	28.07	11300	108.87
4.5	49.36	36.81	10400	142.73
5.5	57.83	45.15	9500	178.76
6.5	67.42	53.56	9000	226.14

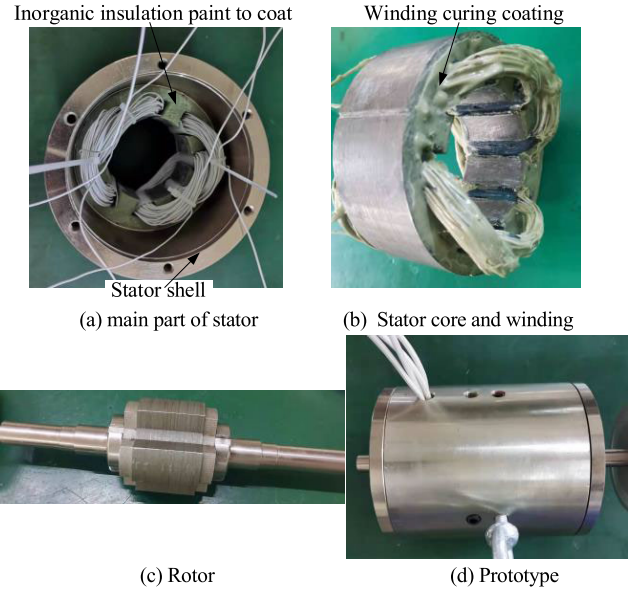


FIGURE 16. HT^o motor prototype.

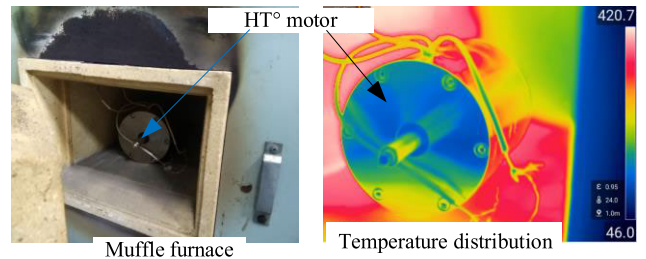


FIGURE 17. High temperature environment test.

be further improved. On the other hand, the improvement of the temperature tolerance limit of the motor can further increase the power density and torque density of the motor.

IV. PROTOTYPE AND EXPERIMENT

In order to further study the application of the MAO ceramic insulated wire to high-temperature motors, a prototype based on it was manufactured. The prototype parameters are shown in Table 1. Due to the high temperature resistance of the motor, its insulation and winding processes are different from traditional motors.

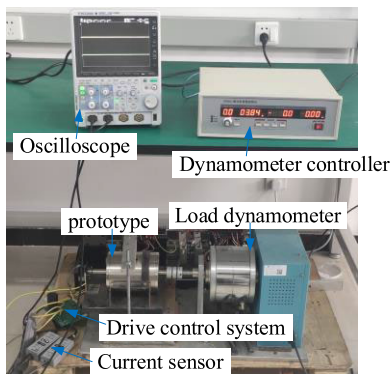


FIGURE 18. Test Platform.

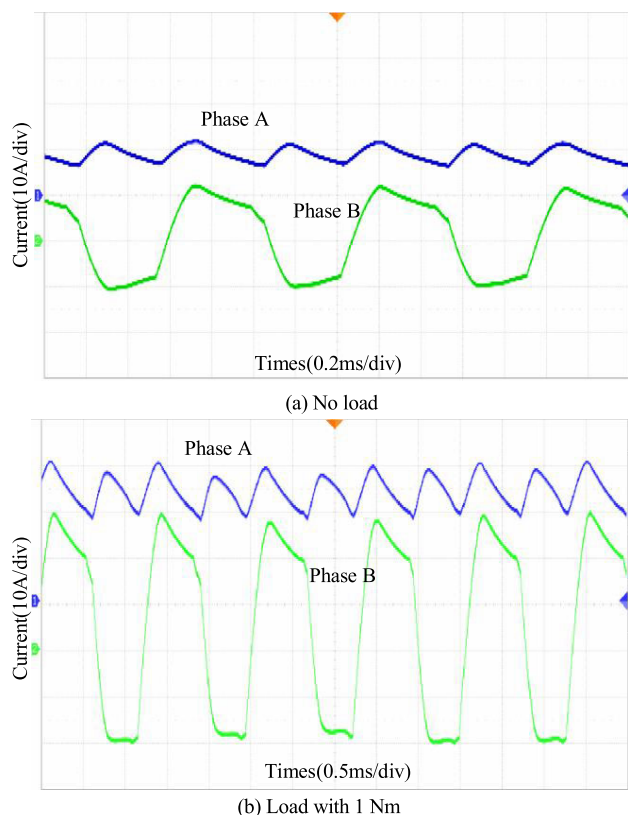


FIGURE 19. The phase current of the motor in different load.

A. ASSEMBLY OF THE HT^o MOTOR AND HIGH-TEMPERATURE RESISTANCE TEST

In order to adapt to high-temperature environments, the insulation of the motor slot is no longer using insulation paper, but using inorganic insulation paint to coat the stator slot to achieve slot insulation of the motor. The winding is also fixed using high-temperature resistant inorganic paint curing method. The stator slot insulation, winding fixation and prototype are shown in Fig. 16.

To verify the high temperature resistance of the motor and its ability to withstand high temperature environments, put the

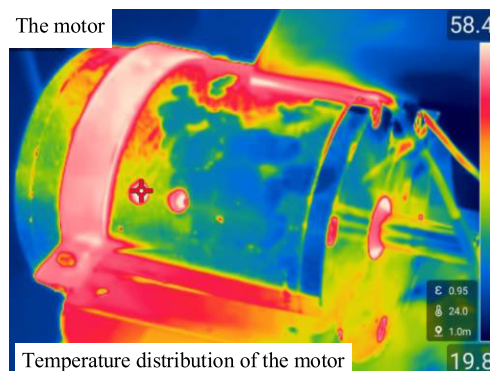


FIGURE 20. The temperature distribution of the motor under the load 1Nm.

motor in a muffle furnace and adjust the furnace temperature to 400 °C for two hours. The muffle furnace and temperature distribution are shown in Fig. 17. After high-temperature baking of the motor, the insulation performance of the motor was not damaged.

B. MOTOR PERFORMANCE TEST AFTER HIGH-TEMPERATURE BAKING

To further verify the high-temperature insulation ability of the motor, the motor performance was tested after high-temperature baking. The test performance is shown in Fig. 18.

220V AC is used to supply the motor drive system, and the drive control system drives the motor. Dynamometer control instrument controls the dynamometer to produce different loads, so that the motor runs in different working conditions. When the dynamometer controller is given A load of 0Nm and 1Nm respectively, the motor speed is 16054 RPM and 11674 RPM respectively. The current waveforms of phase A and B are shown in Fig. 19. When the load is zero, the output torque of the motor mainly overcomes the friction loss and wind resistance loss.

When the motor operates under the load of 1Nm, its steady-state temperature distribution is shown in Fig. 20. From Fig. 20 and Fig. 15(a), the temperature analysis of the motor agrees well with the experimental.

V. CONCLUSION

In this paper, the MAO ceramic insulated wire was proposed for application in motors to achieve a breakthrough in motor operating temperature. The generation conditions, formation principles, structural characteristics and electrical characteristics of MAO ceramic insulated wires were introduced. The breakdown voltage, mechanical strength, high temperature withstand voltage, and service life of ceramic wires were studied in detail to verify their feasibility in motor applications. Verified the insulation characteristics and service life of MAO ceramic insulated wires under high temperature conditions, and met the application conditions in high-temperature motors. The magnetic wire was applied to a high-temperature

motor, the basic structure of the motor was introduced, and the temperature of the motor was simulated. The results showed that when the operating temperature of the motor increased from 75 °C to 226 °C, the motor power increased from 3.3kw to 6.1kw, and the output torque increased from 2.5Nm to 6.5Nm. Finally, a high-temperature motor prototype was made, which was fixed with inorganic insulation paint for winding and slot insulation. Experimental testing was conducted on the temperature resistance performance of the high-temperature motor, and load experiments were conducted to verify the effectiveness of the aforementioned analysis.

REFERENCES

- [1] S. Babicz, S. Ait-Amar, and G. Velu, "Dielectric characteristics of an anodized aluminum strip," *IEEE Trans. Dielectr. Electr. Insul.*, vol. 23, no. 5, pp. 2970–2977, Oct. 2016, doi: [10.1109/TDEI.2016.7736860](https://doi.org/10.1109/TDEI.2016.7736860).
- [2] V. Iosif, D. Roger, S. Duchesne, and D. Malec, "Assessment and improvements of inorganic insulation for high temperature low voltage motors," *IEEE Trans. Dielectr. Electr. Insul.*, vol. 23, no. 5, pp. 2534–2542, Oct. 2016, doi: [10.1109/TDEI.2016.7736810](https://doi.org/10.1109/TDEI.2016.7736810).
- [3] D. Malec, D. Roger, and S. Duchesne, "An electrical machine made with inorganic rigid coils: A breakthrough toward high temperature motors designed for aeronautics," in *Proc. IEEE Electr. Insul. Conf. (EIC)*, Jun. 2018, pp. 1–4.
- [4] M. Schiefer and M. Doppelbauer, "Indirect slot cooling for high-power-density machines with concentrated winding," in *Proc. IEEE Int. Electric Mach. Drives Conf. (IEMDC)*, May 2015, pp. 1820–1825, doi: [10.1109/IEMDC.2015.7409311](https://doi.org/10.1109/IEMDC.2015.7409311).
- [5] S. A. Semidey and J. R. Mayor, "Experimentation of an electric machine technology demonstrator incorporating direct winding heat exchangers," *IEEE Trans. Ind. Electron.*, vol. 61, no. 10, pp. 5771–5778, Oct. 2014, doi: [10.1109/TIE.2014.2303779](https://doi.org/10.1109/TIE.2014.2303779).
- [6] F. Guo and C. Zhang, "Oil-cooling method of the permanent magnet synchronous motor for electric vehicle," *Energies*, vol. 12, no. 15, p. 2984, Aug. 2019, doi: [10.3390/en12152984](https://doi.org/10.3390/en12152984).
- [7] G. C. Montanari and F. J. Lebok, "Thermal degradation of electrical insulating materials and the thermokinetic background: Theoretical basis," *IEEE Trans. Electr. Insul.*, vol. 25, no. 6, pp. 1029–1036, Dec. 1990, doi: [10.1109/14.64487](https://doi.org/10.1109/14.64487).
- [8] F. Aymonino, T. Lebey, D. Malec, C. Petit, J. S. Michel, and A. Anton, "Dielectrics measurements of rotating machines insulation at high temperature (200–400°C)," in *Proc. CEIDP*, Oct. 2006, pp. 740–743, doi: [10.1109/CEIDP.2006.312038](https://doi.org/10.1109/CEIDP.2006.312038).
- [9] S. Babicz and G. Vélú, "Improving insulation quality of ceramic insulated conductors by dip coating with boron oxide," *IEEE Trans. Dielectr. Electr. Insul.*, vol. 26, no. 1, pp. 51–55, Feb. 2019, doi: [10.1109/TDEI.2018.007418](https://doi.org/10.1109/TDEI.2018.007418).
- [10] Z. Wang, R. Freer, L. Fang, and I. Cotton, "Development of low temperature co-fired ceramic (LTCC) coatings for electrical conductor wires," *IEEE Trans. Dielectr. Electr. Insul.*, vol. 23, no. 1, pp. 158–164, Feb. 2016, doi: [10.1109/TDEI.2015.005365](https://doi.org/10.1109/TDEI.2015.005365).
- [11] E. N. Juszczak, D. Roger, K. Komez, M. Lefik, and P. Napieralski, "Architecture choices for high-temperature synchronous machines," *Open Phys.*, vol. 18, no. 1, pp. 683–700, Jan. 2020, doi: [10.1515/phys-2020-0154](https://doi.org/10.1515/phys-2020-0154).
- [12] D. Roger, G. Vélú, S. Ait-Amar, and S. Babicz, "High temperature machines: A comparison between ceramic-coated wires and anodized aluminum strips," *Int. J. Appl. Electromagn. Mech.*, vol. 63, no. 4, pp. 715–724, Aug. 2020, doi: [10.3233/JAE-209209](https://doi.org/10.3233/JAE-209209).
- [13] Y. Pang and S. N. B. Hodgson, "Ceramic/inorganic-organic nano-hybrid composites for thermally stable insulation of electrical wires. Part I: Composition and synthetic parameters," *IEEE Trans. Dielectr. Electr. Insul.*, vol. 27, no. 2, pp. 395–402, Apr. 2020, doi: [10.1109/TDEI.2019.008379](https://doi.org/10.1109/TDEI.2019.008379).
- [14] A. Elmushyakh, "Parametric characterization of nano-hybrid wood polymer composites using ANOVA and regression analysis," *Structures*, vol. 29, pp. 652–662, Feb. 2021, doi: [10.1016/j.istruc.2020.11.069](https://doi.org/10.1016/j.istruc.2020.11.069).
- [15] A. L. Yerokhin, A. Shatrov, V. Samsonov, P. Shashkov, A. Pilkington, A. Leyland, and A. Matthews, "Oxide ceramic coatings on aluminium alloys produced by a pulsed bipolar plasma electrolytic oxidation process," *Surf. Coatings Technol.*, vol. 199, nos. 2–3, pp. 150–157, Sep. 2005, doi: [10.1016/j.surfcoat.2004.10.147](https://doi.org/10.1016/j.surfcoat.2004.10.147).
- [16] L. Zhu, Z. Guo, Y. Zhang, Z. Li, and M. Sui, "A mechanism for the growth of a plasma electrolytic oxide coating on Al," *Electrochimica Acta*, vol. 208, pp. 296–303, Aug. 2016, doi: [10.1016/j.electacta.2016.04.186](https://doi.org/10.1016/j.electacta.2016.04.186).
- [17] L. Zhu, X. Ke, J. Li, Y. Zhang, Z. Zhang, and M. Sui, "Growth mechanisms for initial stages of plasma electrolytic oxidation coating on Al," *Surf. Interfaces*, vol. 25, Aug. 2021, Art. no. 101186, doi: [10.1016/j.surfin.2021.101186](https://doi.org/10.1016/j.surfin.2021.101186).
- [18] Y. Zhang, Y. Wu, D. Chen, R. Wang, D. Li, C. Guo, G. Jiang, D. Shen, S. Yu, and P. Nash, "Micro-structures and growth mechanisms of plasma electrolytic oxidation coatings on aluminium at different current densities," *Surf. Coatings Technol.*, vol. 321, pp. 236–246, Jul. 2017, doi: [10.1016/j.surfcoat.2017.04.064](https://doi.org/10.1016/j.surfcoat.2017.04.064).
- [19] L. Wang, Z. Gao, L. Lei, H. Ma, Y. Geng, Z. Liu, and J. Wang, "Experimental investigation of dielectric breakdown strength and thermal stability of micro-arc oxidation ceramic coating on aluminum winding," in *Proc. 5th Int. Conf. Electric Power Equip. Switching Technol. (ICEPE-ST)*, Oct. 2019, pp. 494–497, doi: [10.1109/ICEPE-ST.2019.8928749](https://doi.org/10.1109/ICEPE-ST.2019.8928749).
- [20] D. Fu, Y. Xu, and Y. Zhang, "Design of low-cost two-phase switched reluctance motor system based on parameters optimization," in *Proc. 18th Int. Conf. Electr. Mach. Syst. (ICEMS)*, Pattaya, Thailand, Oct. 2015, pp. 858–863, doi: [10.1109/ICEMS.2015.7385155](https://doi.org/10.1109/ICEMS.2015.7385155).



WANG LIANKE (Student Member, IEEE) was born in Zhumadian, China, in 1995. He received the B.S. degree in electrical engineering from the China University of Mining and Technology, Xuzhou, China, in 2017. He is currently pursuing the Ph.D. degree in electrical engineering with Xi'an Jiaotong University, Xi'an, China. His current research interests include micro-arc oxidation, ceramic insulated wires, and high temperature motor.



FU DONGSHAN (Member, IEEE) received the B.S. degree in electrical engineering and automation from the School of Information and Electrical Engineering, China University of Mining and Technology, Xuzhou, China, in 2013, and the Ph.D. degree from the School of Electrical Engineering, Shandong University, China, in 2019. From September 2017 to September 2018, he visited Ecole Centrale de Lille, France, as a Joint Ph.D. Student. Currently, he is a Lecturer with the

School of Electrical Engineering, China University of Mining and Technology. His research interests include design and analysis for permanent magnet machines, special structural machines, and new material motors.



WANG XIANGRUI received the B.S. degree in electrical engineering and automation from the Jiangsu University of Science and Technology, Zhenjiang, China, in 2022. He is currently pursuing the M.S. degree with the School of Electrical Engineering, China University of Mining and Technology, Xuzhou, China. His research interests include the simulation design and optimization of electromagnetic devices.



ZHOU YONG is currently pursuing the degree with the School of Electrical Engineering, China University of Mining and Technology. He is also working on the graduation project of optimizing the design of two-phase switched reluctance motors based on new insulation.



SI HONGYU received the bachelor's degree in electrical engineering and automation from the School of Electrical Engineering, China University of Mining and Technology, in 2021, where he is currently pursuing the degree in electrical engineering. His research interest includes switched reluctance motor control topology and algorithms.



GENG YINGSAN (Senior Member, IEEE) was born in Xinxiang, China, in 1963. He received the B.S., M.S., and Ph.D. degrees in electrical engineering from Xi'an Jiaotong University (XJTU), Xi'an, China, in 1984, 1987, and 1997, respectively. He is currently a Professor with the State Key Laboratory of Electrical Insulation and Power Equipment, Department of Electrical Engineering, XJTU. His current research interests include the theory and application of low-voltage circuit breakers and high-voltage vacuum circuit breakers.



LEI LI was born in April 1964. He received the Ph.D. degree in electrical engineering from Xi'an Jiaotong University. He is currently a part-time Professor with Xi'an Jiaotong University, a part-time Professor with Shanghai Jiaotong University, a member of the Global Alumni Association with Xi'an Jiaotong University, and a member of the Professional Committee of Electrical Intelligent Systems and Applications with the Chinese Electrical Engineering Society. He is currently the Executive Director of the Sino-Russian Joint Laboratory and the Sino-Russian (Zhuji) International Laboratory and the General Manager of Sibyli Electric Technology (Suzhou) Company Ltd. His research interests include the research of basic theories and key common technologies in interdisciplinary applications of interface material surface treatment and material body enhancement.



XIANG BO was born in Baoying, Jiangsu, in March 1998. He is currently pursuing the bachelor's degree in electrical engineering and automation with the School of Electrical Engineering, Yangzhou University, in 2023. From 2023 to 2026, he will be a postgraduate majoring in electrical engineering with the China University of Mining and Technology. His research interest includes motor intelligent control technology and its drive system design.

...